

Interstellar Extinction Law toward the Galactic Center IV: J, H, and Ks Bands from VVV Red Clump Stars

Schun NAGATOMO¹, Tetsuya NAGATA¹, and Shogo NISHIYAMA²

¹Department of Astronomy, Graduate School of Science, Kyoto University, Kyoto 606-8502

²Miyagi University of Education, Aoba-ku, Sendai 980-0845, Japan

*E-mail: nagatomo@kustastro.kyoto-u.ac.jp

Received ; Accepted

Abstract

We have determined the wavelength dependence of the extinction in the near-infrared bands (J , H , K_S) toward the Galactic center from the VVV (VISTA Variables in the Vía Láctea) aperture photometry of the stars in the region $|l| \lesssim 2^\circ.0$ and $0^\circ.5 \lesssim |b| \lesssim 1^\circ.0$; this region consists of 12 VVV tiles. We have found significant systematic discrepancy up to ~ 0.1 mag between the stellar magnitudes of the same stars in overlapping VVV tiles. However, by carefully using the positions of red clump stars in color-magnitude diagrams as a tracer of the extinction and reddening, we are able to determine the average of the ratios of total to selective extinction to be $A(K_S)/E(H - K_S) = 1.44 \pm 0.04$, $A(K_S)/E(J - K_S) = 0.423 \pm 0.024$, $A(H)/E(J - H) = 1.25 \pm 0.04$; from these ratios, a steep power law $A(\lambda) \propto \lambda^{-\alpha}$ whose index α is $\sim 2.0 - 2.3$ in the J, H, K_S wavelength range is estimated. The obtained wavelength dependence is consistent with those obtained with the Mauna Kea Observatory (MKO) photometric system employed in the Simultaneous 3-color InfraRed Imager for Unbiased Survey (SIRIUS) camera attached to the Infrared Survey Facility (IRSF) telescope in previous studies. Such a steep decline of extinction toward the longer wavelengths is also in line with recent results based on deep imaging surveys. The determined extinction law seems to be variable in the VVV tile to tile, and it is not clear how much of this is due to real sight line variations and due to observational systematic effects. Thus, there might be room for improvement of the

extinction law determination from the existing VVV data, but this steep extinction law tends to locate heavily reddened objects in the Galactic plane more distant from us when their distance moduli are calculated from the observed reddening values.

Key words: Galaxy: bulge — infrared: stars — dust, extinction

1 Introduction

The clump of red giants (hereafter red clump, RC) is a striking feature in the color-magnitude diagrams (CMDs) of the bulge of the Milky Way Galaxy. The near constancy of intrinsic properties of the RC stars are now widely recognized, and they are employed in the “RC method”, in which candidate RC stars are used as probes of interstellar extinctions and other quantities (Girardi 2016). Following the determination of the total to selective extinction $A(V)/E(V - I)$ by Woźniak & Stanek (1996) and $A(I)/E(V - I)$ by Udalski (2003), Nishiyama et al. (2006; hereafter N06) determined the wavelength dependence of the extinction in the near-infrared bands (J , H , K_S) toward the Galactic center from the observation of RC stars with the Mauna Kea Observatory (MKO) filters (Tokunaga et al. 2002) employed in the Simultaneous 3-color InfraRed Imager for Unbiased Survey (SIRIUS) camera attached to the Infrared Survey Facility (IRSF) telescope (Nagayama et al. 2003).

Nishiyama et al. (2009; hereafter N09) examined the wavelength dependence of the extinction from 1.2 to $8.0\mu\text{m}$ using the Two Micron All Sky Survey (2MASS) and Spitzer/IRAC/GLIMPSE II catalogs. However, these two catalogs are not deep enough to contain all the RC stars. To overcome the limitation, N09 assumed that the center of distribution in the lines of sight is at the same distance from us both for the RC giants and the giants in the upper red giant branch (RGB). They then determined the reddening $E(K_S - \lambda)$ of the upper RGB for the 2MASS and IRAC wavebands while using the IRSF/SIRIUS determination of the extinction $A(K_S)$ of the RC stars. The derived wavelength dependence of the extinction in the 2MASS J , H , and K_S bands showed good agreement with the MKO system. N09 have come to the conclusion that the extinction is well fitted by a power law of steep decrease $A(\lambda) \propto \lambda^{-2.0}$ toward the GC, in contrast to the Cardelli et al. (1989) fit to the Rieke & Lebofsky (1985) result of gentle decrease $A(\lambda) \propto \lambda^{-1.6}$ in the near infrared.

However, there seems to be a slight difference between the derived wavelength dependences from the IRSF/SIRIUS MKO photometric system (with the “pure” RC method) and the 2MASS system (with the RC method variant mentioned above). In particular, the total to selective extinction ratio $A(K_S)/E(H - K_S)$, probably most useful in determining the extinction from the observed reddening

of highly reddened stars, is 1.44 ± 0.01 in the IRSF/SIRIUS MKO system, but it is calculated to be 1.66 ± 0.06 if the $A(H)$ and $A(K_S)$ values for the 2MASS system in Table 1 of N09 are used¹. Dékány et al. (2015a) transformed this larger ratio in the 2MASS system to the VISTA system (Saito et al. 2012) and obtained $A(K_S)/E(H - K_S) = 1.63$, which is then used to determine extinctions and distances of classical Cepheids they discovered in the VISTA Variables in the Vía Láctea (VVV) survey (Minniti et al. 2010). This large ratio implies rather gentle decrease of extinction toward the longer wavelength, although not as gentle as the Cardelli et al. (1989) curve of $A(K)/E(H - K) = 1.83$.

Such a difference can cause a serious discrepancy in determining the distance of objects because the observed color of a reddened object leads to a larger extinction and a smaller distance when a larger ratio (gentler extinction decrease) is adopted. As long as the target objects are not so much reddened by significant dust, the choice of extinction curves does not matter as in the case of type II Cepheids in the VVV survey (Bhardwaj et al. 2017), where only a small fraction of them suffers reddening of $E(J - K_S) > 1$. However, in the case of classical Cepheids, most of them are concentrated to the Galactic plane and suffer heavy extinction; Matsunaga et al. (2016) questioned the distances of the classical Cepheids determined by Dékány et al. (2016a, 2015b), suggested that all their Cepheids are in fact more distant, and disapproved the presence of a putative inner thin disk of young stars represented by Cepheids.

Since the fourth data release (DR4) of the VVV survey is already made public and its photometric catalogue based on aperture photometry (see Saito et al. 2012) is widely used, straightforward determination of the extinction law using these data seems highly desirable. In this paper, we have determined the ratios of total to selective extinction $A(K_S)/E(H - K_S)$, $A(K_S)/E(J - K_S)$, and $A(H)/E(J - H)$ by simply adopting the RC method on the VVV data toward the field observed and analyzed with the RC method by N06, without the assumption of the coexistence of upper RGB stars and RC stars or any transformation between photometric systems. In the process of selecting the RC stars, we have found that there is significant systematic discrepancy up to ~ 0.1 mag in the stellar magnitudes between the aperture photometries of a star in the overlapping VVV tiles. However, averaging the ratio in each tile, we have derived the overall extinction tendency toward the GC.

2 VVV Data and CMD Analysis

We use the VVV DR4 photometric catalogues² which contain calibrated aperture photometry, adopting the “aperture 1” magnitudes with the aperture diameter of 1.0 arcsec (smallest). We determine the

¹ Schultheis et al. (2014) used a ratio $A(K_S)/E(H - K_S) = 1.61$ from the same table by N09, but this is based on the observation of 2MASS H and IRSF/SIRIUS K_S .

² <http://www.eso.org/rm/api/v1/public/releaseDescriptions/80>

ratios of total to selective extinction in the same field as N06. We might be able to exploit the merits of the VVV data and examine a larger field, but we would like to examine exactly the same field as N06 to check the possible differences (due to sites, telescopes, IR imagers, detectors, and filters; see also Soto et al. (2013)) between the IRSF and VVV surveys. First, we divide each square field of $20' \times 20'$ in Figure 1 of N06 (41 in total) of $|l| \lesssim 2^\circ.0$ and $0^\circ.5 \lesssim |b| \lesssim 1^\circ.0$, into 25 subfields of $4' \times 4'$. The VVV data for these fields are from the 12 “tiles” b318-321, b332-335, and b346-349 (Figure 1; see also Fig.2 of Saito et al. (2012) for the designation). Then we construct K_S versus $H - K_S$ CMDs. For selective extinction related with the J band, we use 18 square fields in total and construct K_S versus $J - K_S$, and H versus $J - H$ CMDs. Second, we extract stars in the region of CMDs dominated by RC stars (the rectangular region of the CMD in Figure 2), and the extracted stars are used to make magnitude and color histograms. These histograms have clear peaks, which are then fitted with a Gaussian function.

Due to highly nonuniform interstellar extinction over the whole area of $|l| \lesssim 2^\circ.0$ and $0^\circ.5 \lesssim |b| \lesssim 1^\circ.0$, the RC peaks in CMDs shift from one sight line to another. The peaks shift in the range $13.4 \lesssim K_S \lesssim 14.6$ and $0.4 \lesssim H - K_S \lesssim 1.2$, and therefore we have to shift the CMD region to extract RC stars from subfield to subfield. Following N06, we use only the subfields in which the peak magnitude of RC stars is about more than 0.5 mag brighter than the limiting magnitudes, to avoid problems of unreliable estimates in too reddened fields.

3 Results

Figures 3(left), (middle), and (right) present the K_S versus $H - K_S$, K_S versus $J - K_S$, and H versus $J - H$ CMDs for the whole data tiles. In the figure, each pair of magnitude and color was obtained from each subfield. The solid lines are least-squares fits to the data. Slopes of the fitted lines are listed in the second column of Table 1. The $A(K_S)/E(J - K_S)$ slope (middle; 0.482 ± 0.02) is very similar to that obtained by N06 (see Table1 bottom), but the $A(H)/E(J - H)$ slope (right; 1.72 ± 0.07) is rather large, and the $A(K_S)/E(H - K_S)$ slope (left; 1.30 ± 0.03) is much smaller. Here, the slopes are derived from the principal component analysis. The original CMD is transformed into the coordinates of the first component and the second component, and then the possible error from the horizontal axis is calculated with the least-squares method. Finally, the transformation of the error back to the original color-magnitude coordinates produces the error in the slope.

We notice that the data in these CMDs are significantly more scattered in comparison with those in N06. Also, the data points seem to be in a few streaks; in particular, the H vs. $J - H$ CMD seems to be composed of two or three streaks nearly parallel to, but rather gentler than the

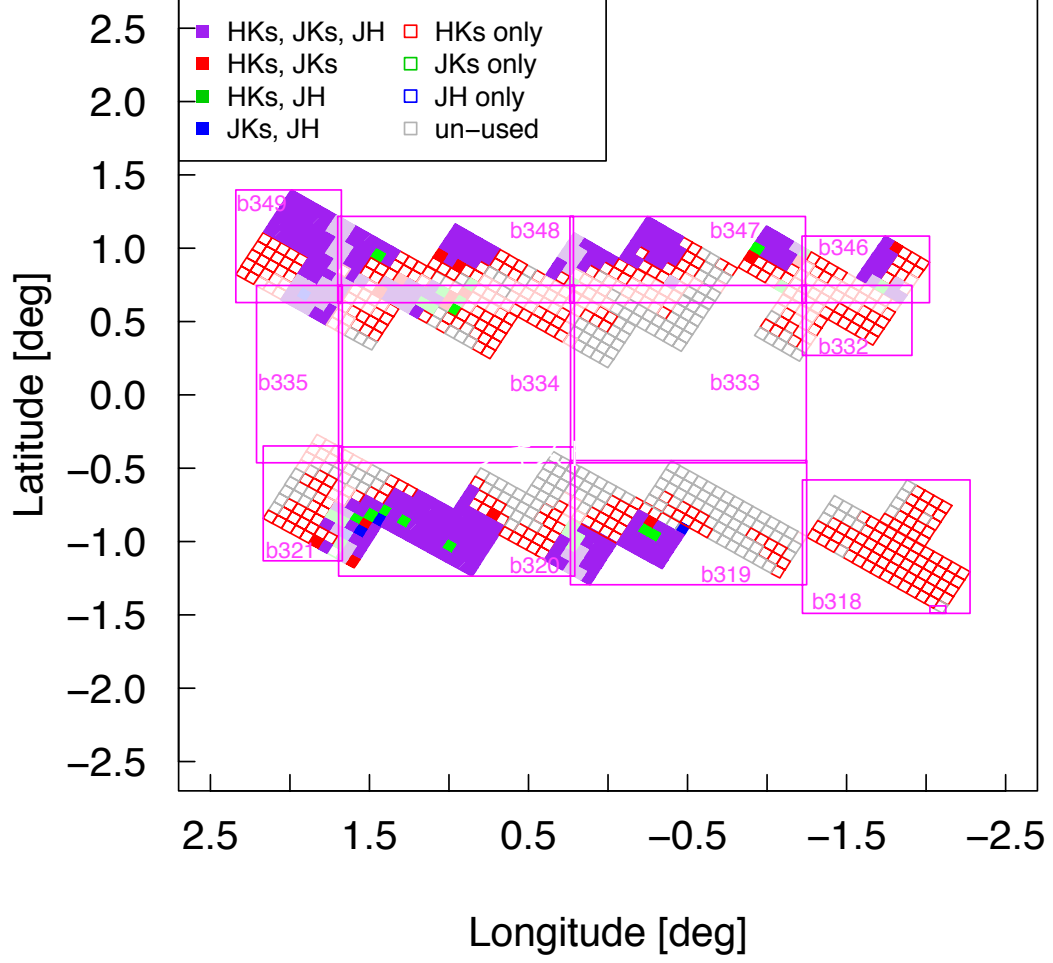


Fig. 1. VVV observation area and fields used for data analysis. The pink rectangle lines are the edges of the 12 VVV tiles in our field analyzed. Following N06, each small square is a subfield of $4' \times 4'$. Only the colored subfields were used for the data analysis in this paper; the gray line squares are the regions where the magnitude and color of RC stars were not reliably determined due to large extinction.

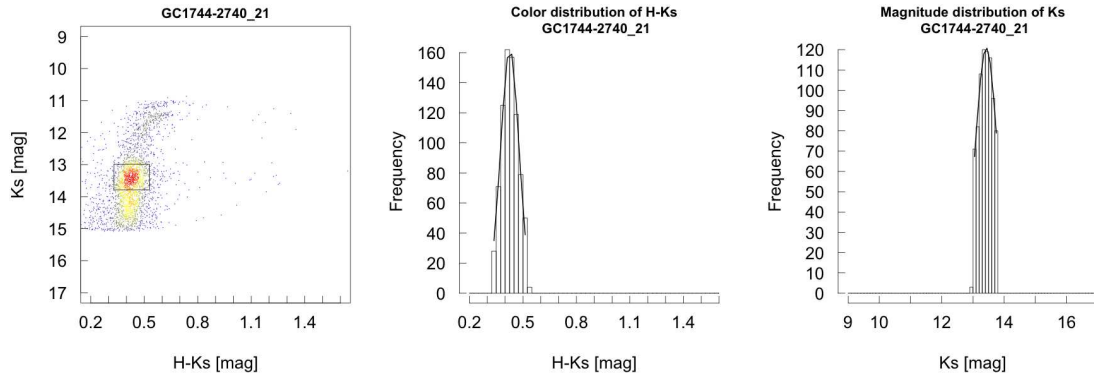


Fig. 2. An example of K_S vs. $H - K_S$ CMD of a subfield (left). In the rectangular region of the left panel, a color peak (middle) and a magnitude peak (right) are determined.

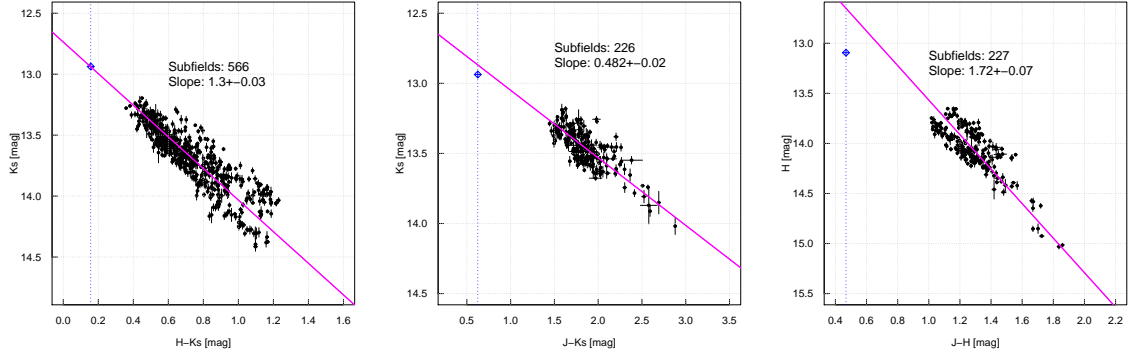


Fig. 3. For the whole data, each magnitude and color Gaussian-fit peaks of RC stars in each subfield K_S vs. $H - K_S$ (left), K_S vs. $J - K_S$ (middle), and H vs. $J - H$ (right) CMDs are shown with the black dots, and the least-squares fits to them (pink lines). The blue squares at the upper left side represent the predicted apparent magnitudes and intrinsic colors of RC stars free from extinction, following Nataf et al. (2016).

fitted line, and the least-squares fit to the data (pink line) passes far above the upper left blue square (the predicted apparent H magnitude and intrinsic $J - H$ color of RC stars free from extinction; see below) because of the several data points in the lower right side. The lower part of the K_S vs. $H - K_S$ CMD also seems to be split. Since the data are taken from the twelve VVV tiles, we plot, for each tile, the K_S vs. $H - K_S$ CMD in Figure 4, the K_S vs. $J - K_S$ CMD in Figure 5, and the H vs. $J - H$ CMD in Figure 6. Each diagram shows definitely smaller scatter; the slope of each fit and the standard deviation of the data points from the fit is shown in Table 1. For instance, the error in the slope in the K_S vs. $H - K_S$ CMD based on all the 566 subfields is 0.03, but the deviation of each subfield point is as large as 0.077. In contrast, if the area is limited to the tile b349, the estimated error in the slope is increased to 0.21 due to the limited $H - K_S$ range (compare Figure 3 (left) and Figure 4 (upper left corner)), but the deviation is reduced to 0.033. Thus, if we calculate the average slope for all the 566 subfields, we get seemingly smaller error estimates in the slopes. However, these subfields are likely to be inhomogeneous and should be analyzed separately.

There seems to be real variation in the sight lines. In fact, it is often suggested that the extinction laws show variations depending on sightlines (N06; Gosling et al. 2009; Nataf et al. 2016). The variation of the extinction law parameter α , when fitted by a power law $A(\lambda) \propto \lambda^{-\alpha}$, is seen on scales as small as 5 arcsec (Gosling et al. 2009). We will examine whether variation in the tile size of \sim a degree really exists or it is due to some systematic observation effects, in the next section. Here, we note that the weighted-mean slopes of the $A(K_S)/E(H - K_S)$ and $A(H)/E(J - H)$ CMDs are more consistent with those obtained by N06. In particular, the $A(K_S)/E(H - K_S)$ slope, which is derived from the maximum number of stars, perfectly agrees with N06.

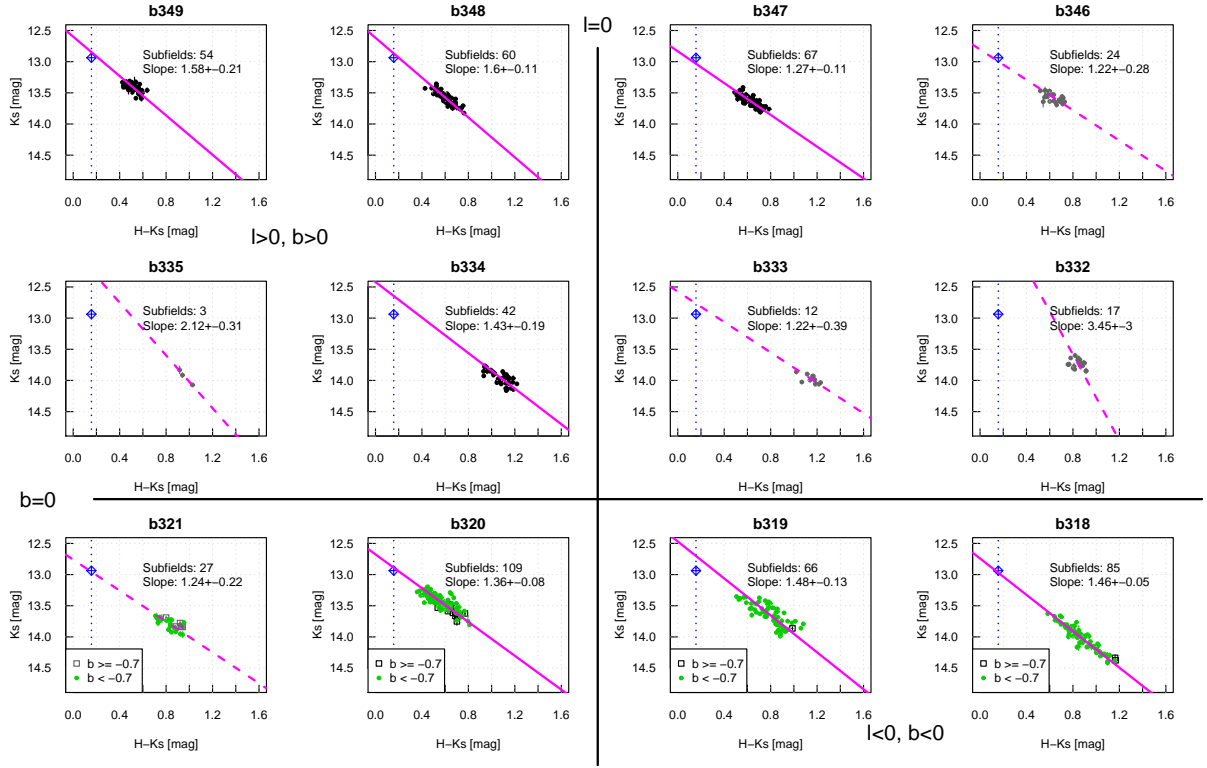


Fig. 4. Each magnitude and color Gaussian-fit peaks of RC stars in the K_S vs. $H - K_S$ CMDs for the VVV tiles $b > 0.7^\circ$ (top), $0.7^\circ > b > 0^\circ$ (middle), and $0^\circ > b$ (bottom). In the bottom diagrams, black squares are $0^\circ > b > -0.7^\circ$, and green dots are $-0.7^\circ > b$ data points. The pink lines are the least-squares fits to the data (Broken lines are poor fits, where less than 5% of total subfields are included in the tile. Their slope errors are significant in general). The upper left blue squares are the predicted apparent K_S magnitude and intrinsic $H - K_S$ color of RC stars free from extinction.

4 Discussion

In the positive Galactic latitude, the slope is smaller at the tiles b333 and b334 closer to the Galactic plane, so we divided the four tiles at the negative Galactic latitude of $|b| = 0.7^\circ$ and listed the slopes of the resultant eight regions in Table 2. The same trend as the positive Galactic latitude might exist in the negative latitude, but it does not seem significant. Rather, the slope seems to show variations in the VVV tile to VVV tile. This might not be surprising because, in the VISTA photometry, after the zero point of the detector is calibrated by the Cambridge Astronomical Survey Unit (CASU) procedure, the transformations between the VISTA and 2MASS systems are determined on a tile by tile basis, and there seems to be an appreciable amount of scatter in them (Soto et al. 2013); this is equivalent to changing the calibration for each tile (see also the CASU website³). We compared the magnitudes of the same stars detected in adjacent VVV tiles, and found small biases. An example is shown in Figure 7; the difference of H magnitudes peaks at -0.07 and $H - K_S$ peaks at -0.11 between the tiles b334 and b348. The influence of such differences is difficult to estimate. For instance, if all the

³ <http://casu.ast.cam.ac.uk/surveys-projects/vista/technical/photometric-properties>

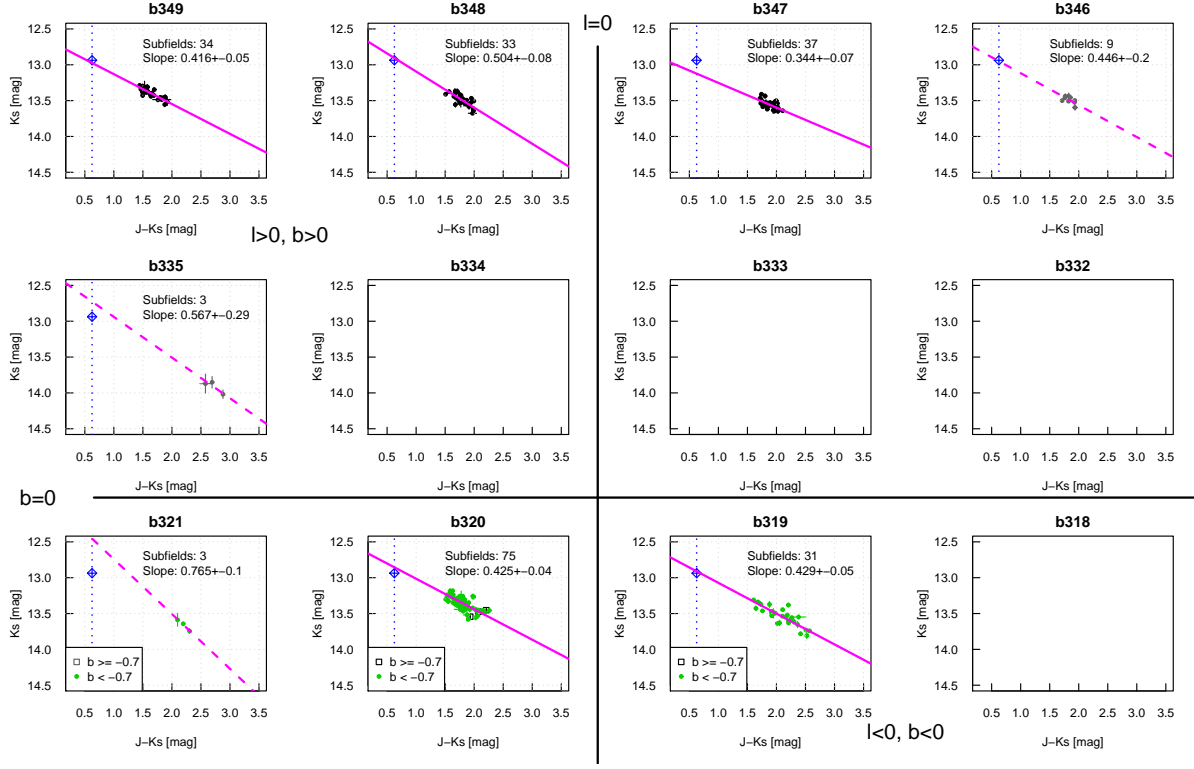


Fig. 5. Same as Figure 4, but for K_S and $J - K_S$. The tiles b332-334 and b318 have no subfields where reliable RC peaks can be determined.

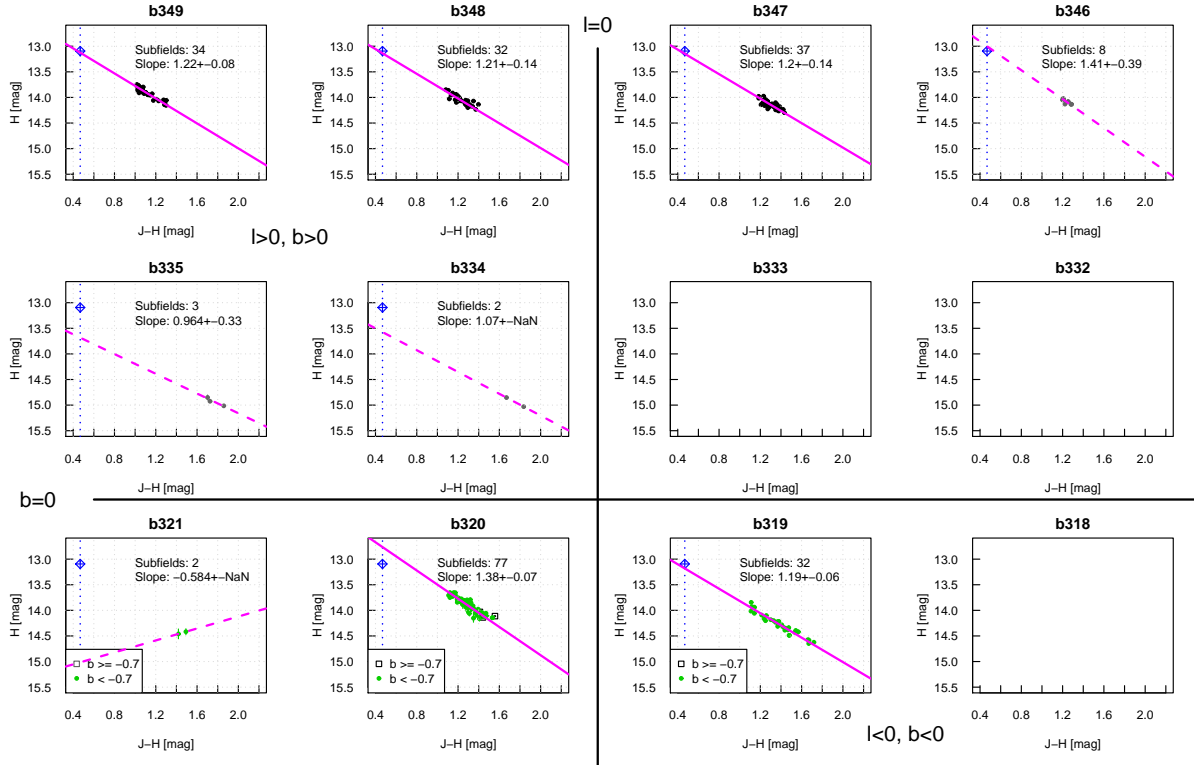


Fig. 6. Same as Figure 4, but for H and $J - H$. The tiles b332, 333, and b318 have no subfields where reliable RC peaks can be determined.

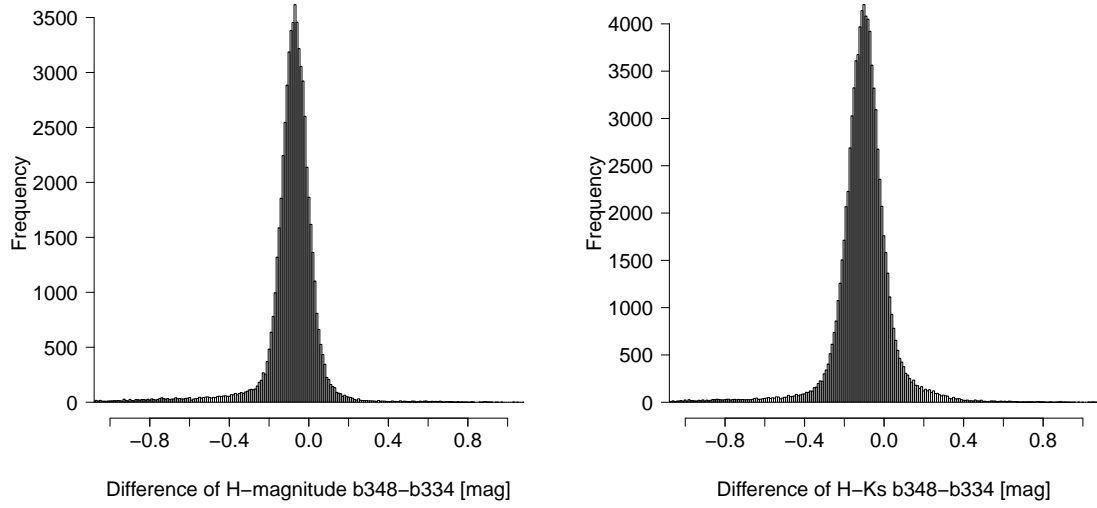


Fig. 7. Difference of H (left) and $H - K_S$ (right) of common stars between the adjacent b334 and b348 tiles. Each bin is 0.01 mag wide.

Table 1. Slopes of the K_S vs. $H - K_S$, K_S vs. $J - K_S$, and H vs. $J - H$ CMDs and deviation from the fits.

Tile	#Subfields	$H - K_S$ Slope	Deviation	#Subfields	$J - K_S$ Slope	Deviation	#Subfields	$J - H$ Slope	Deviation
$b > 0.7^\circ$									
b349	54	1.58 ± 0.21	0.033	34	0.416 ± 0.05	0.033	34	1.22 ± 0.08	0.026
b348	60	1.60 ± 0.11	0.029	33	0.504 ± 0.08	0.045	32	1.21 ± 0.14	0.035
b347	67	1.27 ± 0.11	0.035	37	0.344 ± 0.07	0.035	37	1.20 ± 0.14	0.034
b346	24	1.22 ± 0.28	0.044	9	0.446 ± 0.20	0.044	8	1.41 ± 0.39	0.017
$0.7^\circ > b > 0^\circ$									
b335	3	2.12 ± 0.31	0.006	3	0.567 ± 0.29	0.031	3	0.964 ± 0.33	0.016
b334	42	1.43 ± 0.19	0.048	0	—		2	(1.07)	
b333	12	1.22 ± 0.39	0.037	0	—		0	—	
b332	17	3.45 ± 3.00	0.046	2	(0.969)		2	(4.99)	
$0^\circ > b$									
b321	27	1.24 ± 0.22	0.045	3	0.765 ± 0.10	0.007	2	(-0.584)	
b320	109	1.36 ± 0.08	0.046	75	0.425 ± 0.04	0.058	77	1.38 ± 0.07	0.035
b319	66	1.48 ± 0.13	0.067	31	0.429 ± 0.05	0.064	32	1.19 ± 0.06	0.033
b318	85	1.46 ± 0.05	0.037	0	—		0	—	
(all)	566	1.30 ± 0.03	0.077	226	0.482 ± 0.02	0.074	227	1.72 ± 0.07	0.078)
weighted mean		1.44 ± 0.04			0.423 ± 0.024			1.25 ± 0.04	
N06 Slope		1.44 ± 0.01			0.494 ± 0.006			1.42 ± 0.02	

Table 2. Slopes of the K_S vs. $H - K_S$, K_S vs. $J - K_S$, and H vs. $J - H$ CMDs in the $0^\circ > b$ regions when divided into $0^\circ > b > -0.7^\circ$ and $-0.7^\circ > b$.

Tile	#Subfields	$H - K_S$ Slope	#Subfields	$J - K_S$ Slope	#Subfields	$J - H$ Slope
$0^\circ > b > -0.7^\circ$						
b321	5	1.13 ± 0.39	0	—	0	—
b320	11	1.54 ± 0.57	3	-0.33 ± 0.10	3	0.51 ± 0.76
b319	1	—	0	—	0	—
b318	2	(9.05)	0	—	0	—
$-0.7^\circ > b$						
b321	22	1.40 ± 0.26	3	0.77 ± 0.10	.2	(-0.58)
b320	98	1.31 ± 0.08	72	0.427 ± 0.045	74	1.42 ± 0.07
b319	65	1.50 ± 0.14	31	0.429 ± 0.049	32	1.19 ± 0.06
b318	83	1.49 ± 0.06	0	—	0	—

magnitudes are shifted in one tile compared to another tile, that will not alter the slope in each tile. However, these differences might explain at least part of the tile-to-tile slope variations.

If we fit the $A(J)$, $A(H)$, and $A(K_S)$ by a simple power law $A(\lambda) \propto \lambda^{-\alpha}$, the overall power law index is $\alpha \sim 2.2$, in contrast to the gentle power law $\sim \lambda^{-1.6}$ assumed in Cardelli et al. (1989). Such steep decline of the extinction as this work toward the longer wavelength is also observed for the Galactic center region (Gosling et al. 2009; Nogueras-Lara et al. 2018), the two globular clusters at $l \sim 4^\circ$ and $l \sim 10^\circ$ (Alonso-García et al. 2015), and for $\sim 4 \text{ deg}^2$ area of the inner Milky Way (Nataf et al. 2016). Therefore, a steep extinction law seems to be established very well in the central region of the Milky Way Galaxy. Furthermore, we also note that the H , K_S , and $3.6\mu\text{m}$ extinction toward a distant Cepheid at $l \sim 30^\circ$ and probably another one at $l \sim 20^\circ$ (Tanioka et al. 2017), the extinction toward the cluster Westerlund 1 at $l \sim -20^\circ$ (Damineli et al. 2016), and the infrared extinction ratios to a variety of objects in wider range of the galactic longitudes l ($5^\circ < l < 30^\circ$ in González-Fernández et al. 2014; between $l \sim 27^\circ$ and $l \sim 100^\circ$ in Stead and Hoare 2009; whole inner Galactic disk in Majaess et al. 2016) point to a steep extinction law also in somewhat outer regions.

The variable extinction method determines the dependence of the variation in extinction on the variation in reddening such as $dA(K_S)/dE(H - K_S)$. However, Nataf et al. (2013) claimed that $A(I)/E(V - I) \neq dA(I)/dE(V - I)$ from their derivation of the extinction to the Galactic bulge using their V and I photometry from OGLE-III observations. They were surprised by this result, but reasoned that since the fields in question that are apart a certain angle diverge linearly with distance, the variation is an average of different extinction laws, weighted strongly by the distant locations.

They called this “composite extinction bias”. We examine if such bias exists in our data. We use the intrinsic luminosity parameters of the RC in Nataf et al. (2013) and Nataf et al. (2016), and examine if the lines in the color magnitude diagrams (Figure 3) pass near the intrinsic points (the upper left blue squares). Extrapolating the reddening laws back to $E(H - K_S) = 0$ approximately leads to a reasonable K_S -band intrinsic magnitude of $K_{S,0} = 12.9$; most of the acceptable least-squares fits (solid pink lines) pass near the intrinsic magnitude (within ~ 0.1 mag from blue squares). The other $J - K_S$ vs. K_S and $J - H$ vs. H CMDs show similar results.

In the fields examined by Nataf et al. (2013) of $|b| \approx 5^\circ$, the component of extinction that contributes differentially to different sight lines and the kind of extinction that contributes equally to both sight lines (contributing to $A(I)/E(V - I)$ but not to $dA(I)/dE(V - I)$) are probably of similar strength. Thus it might lead to “an unphysical difference in the value of $I_0 = 0.24$ mag” (Nataf et al. 2013). In our fields of $|b| \approx 1^\circ$, however, the main contributor exists in the distant part, and its various parts are nearly equally apart. Therefore, $A(K_S)/E(H - K_S) \simeq dA(K_S)/dE(H - K_S)$ seems to hold.

Since a new PSF photometry of the VVV images is available (Alonso-García et al. 2018) and provides more detection in the most crowded regions surveyed by VVV, we examined the PSF photometry magnitudes of the stars in the aperture photometry catalog. In all the area of this study, the aperture photometry catalog (vvvSource) and the PSF photometry catalog (vvvPsfDophotZYJHKsSource) were compared. We used only the entries whose magnitude errors are less than 0.1 mag in both the catalogs and one-to-one matches are guaranteed. The comparison was made tile by tile. It is not surprising that the agreement of magnitudes is generally very good because the PSF photometry also “relies heavily on the astrometric and photometric solutions provided by CASU” (Alonso-García et al. 2018); it is calibrated with the aperture photometry and brought to the VISTA photometric system. However, the medians of differences in some corresponding tiles was found to exceed 0.05 mag. Therefore, we have estimated the influence of such magnitude differences to the resultant slopes in the color magnitude diagrams; the influence seems to be insignificant. Thus, our results are likely to hold for the new VVV PSF photometry also.

Then, what caused the difference in the extinction law derived here and those in Alonso-García et al. (2017), who made use of PSF photometry of VVV data? Their measured ratios of total to selective extinction were $A(K_S)/E(H - K_S) = 1.104 \pm 0.022 \pm 0.2$, which is significantly different from our ratio 1.44, and $A(K_S)/E(J - K_S) = 0.428 \pm 0.005 \pm 0.04$, which is rather similar to ours 0.423. The first cause of the difference would be that they use the VVV data obtained at smaller Galactic latitudes, thanks to the deeper PSF photometry. As shown above and in Figure 3 of Alonso-García et al. (2017), the extinction laws show variations depending on sightlines. If the ratio $A(K_S)/E(H - K_S)$ is smaller near the Galactic plane, it might explain the difference. Another

possibility is the slight differences in analysis. Alonso-García et al. (2017) used the whole area CMDs. They divided them into narrow sections of color, generated histograms of the stars in each color bins, and fitted the histograms with a second-order polynomial function plus two Gaussians representing the RC and other stars. The RC stars seem to be separated well, and the Gaussian fitting results were used to derive their extinction law. In contrast, we have selected a rectangle region that is supposed to be occupied only by the RC stars in each CMD, taken from each subfield, and fit the magnitude and color distributions with a Gaussian function. We made such procedures to select only the RC stars in the bulge, because other various components in the foreground and background (e.g., Alonso-García et al. 2018 and González et al. 2018) can contaminate. Furthermore, the tile-to-tile photometry difference found here might have complicated the whole area CMDs; our average slopes for all area CMDs are different from the mean values of each tile.

5 Summary

The average of the ratios of total to selective extinction derived from the VVV aperture photometry of RC stars $A(K_S)/E(H - K_S) = 1.44 \pm 0.04$, $A(K_S)/E(J - K_S) = 0.423 \pm 0.024$, $A(H)/E(J - H) = 1.25 \pm 0.04$ are similar to those obtained from RC stars with the IRSF/SIRIUS system in previous studies. This steep extinction law has been found to be also typical of recent deep imaging towards the inner Galaxy. This extinction law is steeper than the classical ones (Rieke & Lebofsky 1985; Cardelli et al. 1989) based on less deep observations, and is in line with recent results based on deep imaging surveys (Nataf et al. 2016; Damineli et al. 2016). In the near infrared, this implies smaller $A(K_S)$ and larger distances, which has a strong impact on inner Galaxy studies.

This work was partly supported by the Grants-in-Aid Scientific Research (C) 21540240, (A) 18H03719, 18H05441, the Global COE Program “The Next Generation of Physics, Spun from Universality and Emergence” from the Ministry of Education, Culture, Sports, Science and Technology (MEXT) of Japan, and the “UCHUGAKU” project of the Unit of Synergetic Studies for Space, Kyoto University. Nishiyama acknowledges support by JSPS KAKENHI, Grant-in-Aid for Challenging Exploratory Research 15K13463, 18K18760, and Grant-in-Aid for Scientific Research (A) 19H00695.

References

- Alonso-García, J., et al., 2015, *AJ*, 149, 99
Alonso-García, J., et al., 2017, *ApJL*, 849, L13

Alonso-García, J., et al., 2018, A&A, 619, A4

Bhardwaj, A., et al., 2017, A&A, 605, A100

Cardelli, J. A., Clayton, G. C., & Mathis, J. S. 1989, ApJ, 345, 245

Damineli, A., Almeida, L. A., Blum, R. D., Damineli, D. S. C., Navarete, F., Rubinho, M. S., Teodoro, M., 2016, MNRAS, 463, 2653

Dékány, I. et al. 2015a, ApJL, 799, L11

Dékány, I. et al. 2015b, ApJL, 812, L29

Girardi, 2016, Annu. Rev. Astron. Astrophys. 54, 95

González-Fernández, C., Ramos, A. A., Garzón, F., Cabrera-Lavers, A., and Hammersley, P. L. 2014, ApJ, 782, 86

González, O. A. et al. 2018, MNRAS, 481, L130

Gosling, A. J., Bandyopadhyay, R. M., & Blundell, M. 2009, MNRAS, 394, 2247

Majaess, D., Turner, D. G., Dékány, I., Minniti, D., & Gieren, W. 2016, A&A, 593, A124

Matsunaga, N., Feast, M. W., Bono, G., et al. 2016, MNRAS, 462, 414

Minniti D. et al., 2010, New Astron., 15, 433

Minniti D. et al., 2017, AJ, 153, 179

Nagayama, T., et al. 2003, Proc. SPIE, 4841, 459

Nataf, D. M. et al. 2013, ApJ, 769, 88

Nataf, D. M. et al. 2016, MNRAS, 456, 2692

Nishiyama, S., et al. 2006, ApJ, 638, 839 (N06)

Nishiyama, S., et al. 2009, ApJ, 696, 1407 (N09)

Nogueras-Lara, F., et al. 2018, A&A, 610, A83

Rieke, G. H., & Lebofsky, M. J. 1985, ApJ, 288, 618

Saito, R. K. et al. 2012, A&A, 537, A107

Schultheis M. et al., 2014, A&A, 566, A120

Soto, M. et al. 2013, A&A, 552, A101

Stead J. J., Hoare M. G., 2009, MNRAS, 400, 731

Tanioka, S., Matsunaga, N., Fukue, K., Inno, L., Bono, G., & Kobayashi, N. 2017, ApJ, 842, 104

Tokunaga, A. T., Simons, D. A., & Vacca, W. D. 2002, PASP, 114, 180

Udalski, A. 2003, ApJ, 590, 284

Woźniak, P. R., & Stanek, K. Z. 1996, ApJ, 464, 233